Clays and Clay Minerals, Vol. 43, No. 6, 682–692, 1995.

FORMATION OF AUTHIGENIC ILLITE IN PALAEOCENE MUDROCKS FROM THE CENTRAL NORTH SEA: A STUDY BY HIGH RESOLUTION ELECTRON MICROSCOPY

JENNIFER M. HUGGETT

Department of Geology, Imperial College, London, SW7 2BP, U.K.

Abstract—The mode of growth of authigenic, lath-shaped illitic particles has been investigated using field emission scanning electron microscopy (FESEM) and high resolution transmission electron microscopy (HRTEM). Two types of clay lath have been identified: overgrowths on platelets of illite or illite-smectite and discrete particles. Both are neoformed and show a slight increase in abundance with depth over the 70 m depth interval sampled. Interpretation of lattice fringe data is not unambiguous but indicates that the clay is either illite or illite-smectite with R1 structure. The formation of discrete particles of authigenic illite, or even R1 illite-smectite, is compatible with present burial depths and a regional geothermal gradient of approximately 40°C/km. This illite also differs from many previous reported occurrences of authigenic illite in mudrocks in that it appears to have formed, without being preceded by progressive illitization of illite-smectite.

Key Words—Authigenic illite, High resolution electron microscopy, Illite-smectite.

INTRODUCTION

Since the publication of the classic paper by Hower *et al* (1976) the smectite to illite transition has become a major focus for clay mineral research. With X-ray diffraction (XRD) as the principal investigative tool, the result has perhaps inevitably, been that trends in expandability with depth have been a key means by which the process has been studied. XRD studies have been supplemented by direct observation of the clay by transmission electron microscopy (TEM) (Ahn and Peacor 1986; Yau *et al* 1987; Amouric and Olives 1991). Concurrently, but quite separately, scanning electron microscopy (SEM) has been used to demonstrate the precipitation of authigenic illite in sandstones (Ehrenberg and Nadeau 1989; Glassman 1992). Perhaps as a consequence of the different approaches used, it has often been tacitly assumed that the mechanisms of illite formation are lithology dependent. It is often assumed that neoformation is dominant in sandstone and either or both transformation and neoformation occur in mudrock. In the present paper, XRD, high resolution field emission SEM (FESEM), and high resolution TEM have been used to investigate the nature of both illite and illite-smectite in interbedded sandstone and mudrock. By examining the two lithologies with the same techniques, it has been possible to directly compare the clay minerals present and their possible mode of origin.

SAMPLES

The sampled well is located in the central North Sea (U.K. sector). Mudrock and sandstone samples were obtained from the sandstone-dominated Forties Sandstone Member of the Sele Formation (Paleocene), over an 88 m depth range, from 2204–2292 m. Present burial depths are also maximum burial depths and the regional geothermal gradient is approximately 40°C/km. Average reservoir temperature over the sampled depth interval is 107°C. The Forties Member is a sandstone dominated turbidite sequence with mudrock beds of variable thickness (5 cm to >1 m).

METHODS

Whole-rock and <4 μm clay fraction XRD analyses were carried out on 31 mudrock and 11 sandstone samples. The <0.2 μm was analyzed (after acid treatment to remove chlorite) from 3 samples from the top, middle and base of the cored interval. The sample preparation, operating conditions used and methods for semi-quantitative determinations of mineral components are described in Huggett (1992). Petrographic data for sandstones (40 samples) were derived from an unpublished report and from Huggett and Isaac (in press), plus 6 thin sections examined specifically for this study.

Fresh fracture surfaces were platinum-coated for examination in a Jeol 6400F field emission SEM (FESEM). Qualitative EDS analyses were carried out using an Oxford Instruments high purity germanium detector with Moran Scientific software. Samples for TEM were prepared by ion-beam milling and by ultra-microtomy. The samples for ion-milling were cut from 30 μm thick sections cut normal to bedding so that the phyllosilicate {001} was preferentially orientated parallel to the electron beam. Samples for ultra-microtomy were imbedded in medium hard resin and sectioned using a Reichert Jung Ultracut E. Duplicate microtomed samples from several depths were prepared by the method devised by Tessier (Środón *et al* 1990).

TEM samples were examined in a Jeol 4000FX TEM. Selected-area electron diffraction patterns could not be obtained from many of the single crystals because of their small grain size. Semi-quantitative EDS analyses were carried out using a Philips T200 equipped with an Oxford instruments AN10000 X-ray analytical system.

RESULTS

Sandstone petrography

The sandstones are quartz-dominated with subordinate amounts of feldspar, rock fragments and clay matrix. Other detrital components include biotite (variably altered), muscovite, heavy minerals, bioclasts, glauconite, tuff fragments, carbonaceous material and very rare chlorite grains. Quartz (40–60%) is predominantly monocrystalline. K Feldspar is generally the second most abundant grain type (2–11%, mean = 6.3%). Plagioclase (<6%, mean = 3.4%) is predominantly Ab-rich with minor partially albitized An-rich plagioclase. It is not clear whether the albitization occurred before, or during, diagenesis. Plagioclase decreases slightly with depth, whereas K feldspar shows no depth trend. The plagioclase is predominantly Ab-rich. Rock fragments constitute up to 13% of the rock and comprise mainly granite and mudrock clasts. Matrix clay (mostly detrital illite and illite-smectite) forms a variable proportion of the sandstones, with a maximum of 29% point counted. XRD data shows no depth trend in the proportions of illite or illite-smectite. On average <0.5% of the porosity was generated by feldspar leaching, and <2% through rock fragment leaching. The principal authigenic minerals in the sandstones are kaolinite, ferroan calcite, siderite, and quartz overgrowth. They are concentrated at a few specific horizons and individually constitute <3% of the rock. Trace amounts of short, lath-shaped authigenic clay are associated with detrital illitic clay and chlorite (Figure 1). Rare calcite, halite, feldspar overgrowths, titanium oxides, pyrite, and limonite/haematite are also present.

Mudrock petrography

XRD data indicate that the mudrocks are mineralogically variable with no overall depth trend. Clay minerals constitute approximately 60% of the mudrocks and are predominantly illite and illite-smectite (40–70% of the clay fraction, 15–30% of the bulk rock), plus kaolinite (25–45% of the clay fraction, 15–20% of the bulk rock), chlorite (5–15% of the clay fraction, 5–10% of the bulk rock), and rare chlorite-smectite (Figure 2a). Chlorite in the mudrocks is predominantly silt-size detrital particles.

Estimates of the illite-smectite composition were obtained by measuring the position of the glycol-treated 002/003 reflection after peak fitting (using the Philips PC APD software) to remove the effect of the discrete illite component. This is a modification of the method in Środón (1980). This method yields estimated values of 40–50% regularly interstratified smectite layers in all but the two most deeply buried samples (from 2271 m and 2271.9 m) which have estimated values of 25% regularly interstratified smectite layers. The proportion of illite to illite-smectite in the <0.2 μm fraction is higher than in the <4 μm fraction, making it harder to determine the proportion of smectite interlayers (Figure 2b). Estimates based on the position of the 002/003 reflection after peak fitting indicate an illite-rich composition (≤20% smectite) for all three <0.2 μm fraction samples. The profiles for all samples were smoothed and checked against calculated profiles (Reynolds and Hower 1970; Reynolds 1985). These yielded results within the same range as the modified Srodon method. XRD data for other wells in the same field (unpublished oil company data) indicate that there is no correlation between illite-smectite composition and depth, or between illite-smectite composition and depth of the diffuse oil-water contact zone. The illite-smectite has therefore been interpreted as detrital.

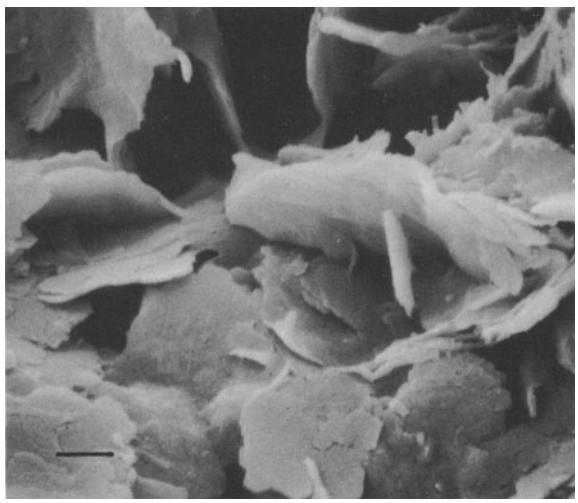

Figure 1. FESEM image of ragged illite or illite-smectite plates, a few have lath-shaped overgrowths. Scale bar = 0.5 μm.

In order of abundance, non-clay minerals present in the mudrocks are: quartz, plagioclase (predominantly Ab-rich, same comments apply as to sandstone plagioclase), K feldspar, minor lithic grains (schist, chert and polycrystalline quartz fragments), phyllosilicates (phengite and minor muscovite), chlorite, pyrite, rare calcite, siderite, cristobalite and organic matter. The proportion of K feldspar semi-quantitatively determined from XRD data (reinforced by estimates from BSEM images) is 0–13% (mean = 3.3%), approximately half the amount in the interbedded sandstone. The proportion of leached K feldspar estimated from BSEM

https://doi.org/10.1346/CCMN.1995.0430604 Published online by Cambridge University Press

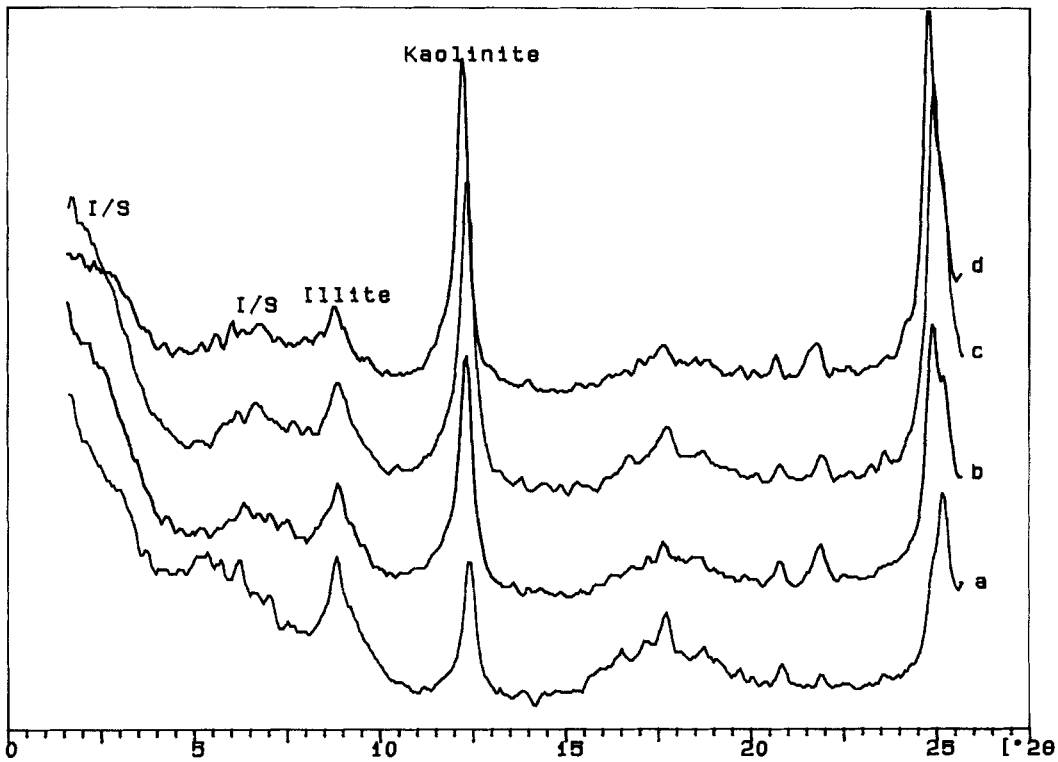

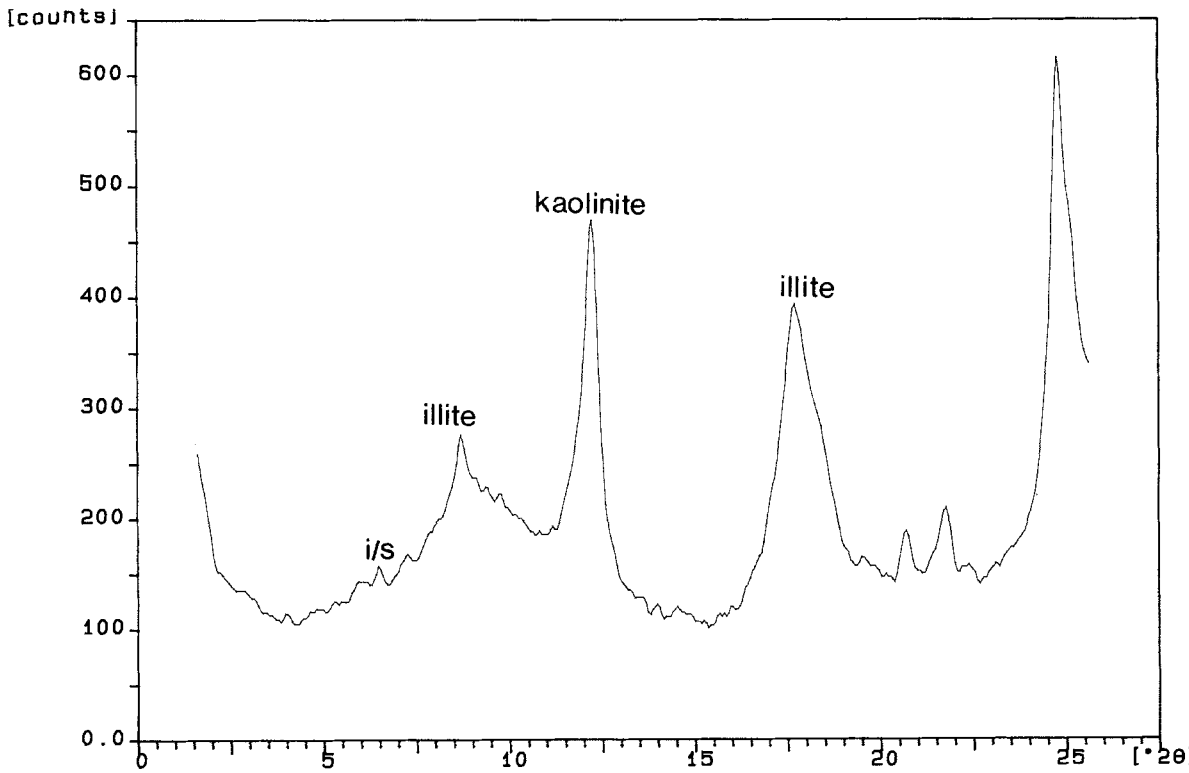

Figure 2a. <4 μm fraction XRD profiles after glycolation: a) 2222.6 m, b) 2249.4 m, c) 2250.6 m, d) 2271.9 m.
Figure 2b. <0.2 μm fraction XRD profiles after glycolation, sample depth is 2233.5 m.

https://doi.org/10.1346/CCMN.1995.0430604 Published online by Cambridge University Press

images is about the same as point counted in sandstone thin sections, <0.5%. The proportion of Ab-rich plagioclase semi-quantitatively determined from XRD data (and reinforced by estimates from BSEM images) is 0–12%, the mean value = 4.6%, the quantity of Ab-rich plagioclase is the same, or slightly more than in the sandstones. Feldspar is characteristically fresh but fractured; the rare corroded grains may have experienced pre-depositional sericitization which predisposes them to being leached during subsequent diagenesis.

Interpretation of HRTEM and FESEM data

The distinction between illite and smectite layers in HRTEM images is crucial to an interpretation but it is not always an easy distinction to make. Experience and computer simulation results (Guthrie and Veblen 1989, 1990; Veblen *et al* 1990) indicate that illite-smectite ordering should only be apparent under very particular conditions of crystal orientation, crystal thickness and microscope focus, if the expandable layers have not been fixed at >1 μm. In ion-beam milled thin foils and conventionally microtomed samples, smectite layers often have a basal spacing of 1 nm due to dehydration during sample preparation. Smectite could only be identified where collapse was intermittent along the entire length of the layer, or with more circumspection, from the undulose, thin, relatively short nature of illite-smectite particles (Vali and Köster 1986; Ahn and Peacor 1986). Dark fringes in under-focused images are tentatively correlated with smectite interlayers (Veblen *et al* 1990; Vali and Köster 1986). Under-focusing may permit the 2 nm periodicity of R1 illite-smectite to be observed (Guthrie and Veblen 1989, 1990; Veblen *et al* 1990) but the 2 nm periodicity is also characteristic of 2M mica. The distinction between the two minerals needs to be made using additional textural and chemical data or knowledge of the pressure/temperature at which the mineral formed.

Microtomed samples prepared by the method of Tessier (Środón *et al* 1990) preserve the 1.25–1.5 nm smectite fringes intercalated with 1 nm fringes in illite-smectite. In these samples S/(S + I) ratios could be reliably measured by counting 1 nm and ~1.3 nm fringes. In conventionally microtomed samples, fringes with periodicities 1.05–1.2, partially collapsed, were occasionally observed (Figure 3). The only distinction between the layer types was a difference in contrast. For these samples S/(S + I) ratios were calculated by counting dark and pale grey fringes. This is not straightforward for many images, particularly where contrast between light and dark fringes is slight. Therefore only high contrast fringes were counted.

Where 0.45 nm cross-fringes occur with 001 fringes, a two-dimensional structure image is produced (Buseck and Ijima 1974). The implication of these fringes is that the rotation of adjacent layers is not random, the

Figure 3. Lattice fringe image of illite-smectite platelet with a lath nucleated at a defect on the platelet surface (open arrow). An ISISISIISIISIS sequence is visible between the solid arrows. The sample is from 2271.9 m and was prepared by the method of Tessier (described in Środon *et al* 1990), the smectite layers have been fixed at approximately 1.3 nm, the illite layers are 1 nm. Scale bar = 8 nm.

illite layers are coherently stacked and are not turbostratic. In this study 0.45 nm cross-fringes were frequently observed, both alone and with 001 fringes (Figure 4a). The stacking pattern is invariably disordered (Figure 4b).

Abundant structural defects within particles have often been interpreted as an indication of a detrital (Baños *et al* 1983; Ahn and Peacor 1986) or low temperature origin (Lee *et al* 1985), while Vali and Köster (1986) related defect density to octahedral and tetrahedral substitution in 2:1 layer silicates. However, illite crystal growth may have been propagated at screw dislocations, in accordance with the BCF theory of spiral growth on crystal faces (Burton *et al* 1951). Consequently the use of structural defects to distinguish between authigenic and detrital illite has not been used in the present study, though the scarcity of defects within the relatively large (>2 μm long) mica particles also present in these samples may indicate a metamorphic, i.e., detrital origin. Most undulose particles and megacrystals contain a few step dislocations or layer defects (Figure 5).

In FESEM images (Figure 6), a detrital origin for most of the illite and illite-smectite is tentatively inferred from the ragged appearance of the flat to undulose platelets. This inference is supported by the absence of any regional correlation between illite-smectite composition and depth, or the position of the oil-water contact (unpublished oil company data). From comparison of the clay morphologies observed here with published SEM data (O'Brien and Slatt 1990; Keller *et al* 1986; Huggett 1989) the flat particles are tentatively identified as illite and the undulose ones as illite-smectite. The qualitative EDS analyses indicate K, Al, Si, minor Mg, and variable but small concen-

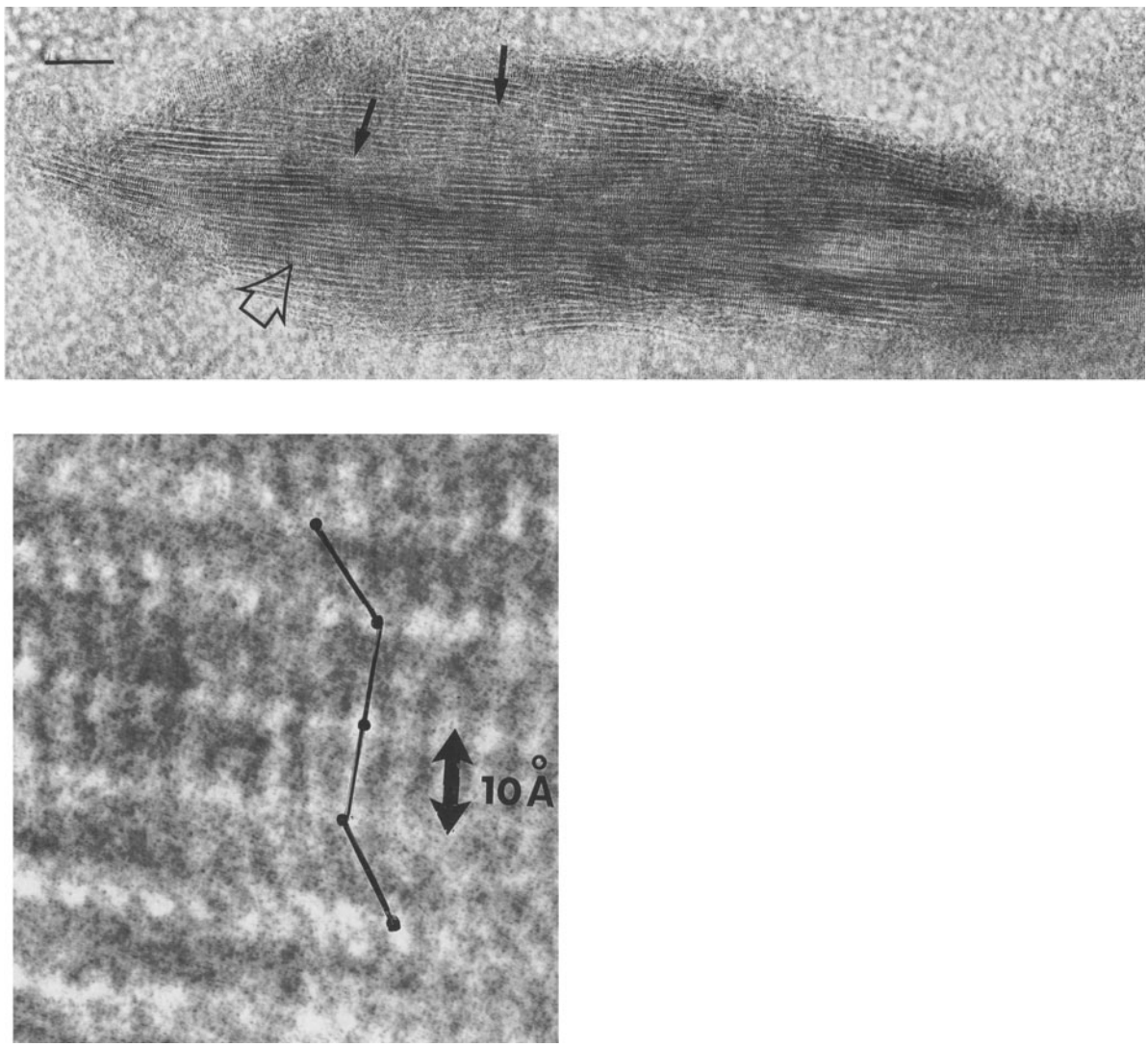

Figure 4a. Structure image of a megacrystal consisting of interleaved packets of clay, mostly 3–5 layers thick, all with 1 nm spacing. Packet margins are defined by growth defects (e.g., solid arrows), the numerous 0.45 nm cross fringes (open arrow) indicate lattice continuity between packets. The sample is from 2249.4 m and was prepared by ultramicrotomy without fixation of expandable layers. Scale bar = 10 nm. b. Detail of area shown immediately above open arrow in Figure 5a. The crystal shows overall 1Md structure, individual packets have 1 M structure.

trations of Na. These data confirm that the clay includes illite but is insufficiently quantitative to distinguish between illite and illite-rich illite-smectite. Where diagnostic fringes were not obtained in HRTEM images, the same tentative rule was applied as for SEM observations: parallel fringes are assumed to be illite, and anastomosing to be illite-smectite (Inoue *et al* 1987, 1988; Peacor 1992; Vali and Köster 1986). TEM images of "illitic" clay in the mudrocks reveal a mass of sub-parallel packets intersecting at low angles, with the layers of one packet terminating against another along part of its length (Figures 4 and 5). The packets within these megacrystals (terminology of Ahn and Peacor 1986) may consist of parallel or anastomosing, wavy fringes. The observation of 0.45 nm cross-fringes indicates that at least some packets in megacrystals are in lattice continuity (Figure 6).

Within each sample by HRTEM, there is a spread of illite-smectite compositions that are only regularly interstratified over a few unit cells. However the modal composition is the same or very close to that determined by interpretation of XRD data: R1 superlattice structures were mostly identified in samples for which XRD indicated regular illite-smectite with 40–50% smectite (Figure 7), and R3 structures were almost exclusively identified in microtomed sections of the two

https://doi.org/10.1346/CCMN.1995.0430604 Published online by Cambridge University Press

Figure 5. Lattice fringe image of a megacrystal consisting of interleaved packets of clay, mostly 5–10 layers thick, all with 1 nm spacing. Packet margins are defined by growth defects (e.g., open arrows). Step dislocations (black arrows) within packets are also present. The sample is from 2266.1 m and was prepared by ultramicrotomy without fixation of expandable layers. Scale bar = 6 nm.

Figure 7. Lattice fringe image with 2 nm spacing throughout. The particles have been bent, possibly during compaction (black arrows). Cross fringes (between the open arrows) indicate lattice continuity. The sample is from 2222.6 m and was prepared by ultramicrotomy without fixation of expandable layers. Scale bar = 5 nm.

deepest mudrock samples for which XRD indicated regular illite-smectite with 25–35% smectite (Figure 3). It is not clear why the XRD data indicate that the bulk of the interstratifications are regular and of narrow compositional ranges, whereas the HRTEM data indicate a similar bulk composition but homogeneity on a fine scale is unlikely to be detected by XRD.

Visual estimates from FESEM images suggest a maximum of 1–2% lath-shaped clay, with an overall increase with depth. Both discrete particles and "overgrowths" on platelets were commonly observed in FESEM images, though the latter predominate (Figure 8). Most clay laths observed by TEM occur as discrete particles 2–10 nm thick, however lattice fringes of laths in crystallographic continuity with illite plates show that the laths may also have either nucleated at, or have "peeled off" from plates where lattice defects (Figure 9) emerge on the plate surface. These laths may correspond to the laths projecting from platelets observed in FESEM images (Figure 8). The higher proportion of discrete laths may be a consequence of "overgrowth" laths having broken off from platelets during sample preparation. The discrete clay laths in TEM images have a high proportion of face to edge contacts (Figure 10), but if the laths are broken, this is not significant. The laths are entirely free from deformation and internal layer terminations. Approximately 50% of them have a 2 nm periodicity, though even in microtomed samples, smectite layers were not observed.

The laths are interpreted as authigenic on account

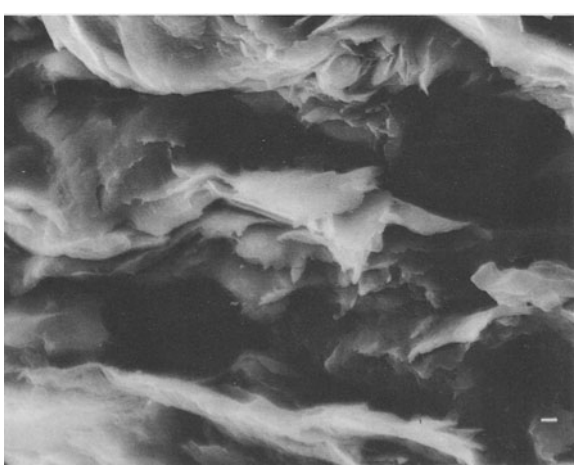

Figure 6. FESEM image of ragged and compacted illite plates, a few have incipient laths. Scale bar = 0.5 μm.

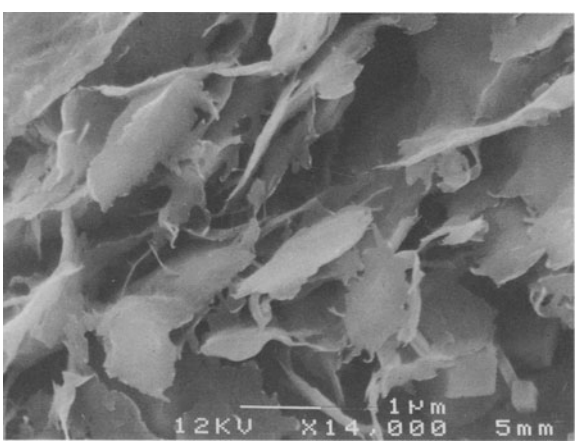

Figure 8. FESEM image of illite/illite-smectite platelets with delicate lath shaped overgrowths. The cubic mineral is pyrite. Scale bar = 1 μm.

https://doi.org/10.1346/CCMN.1995.0430604 Published online by Cambridge University Press

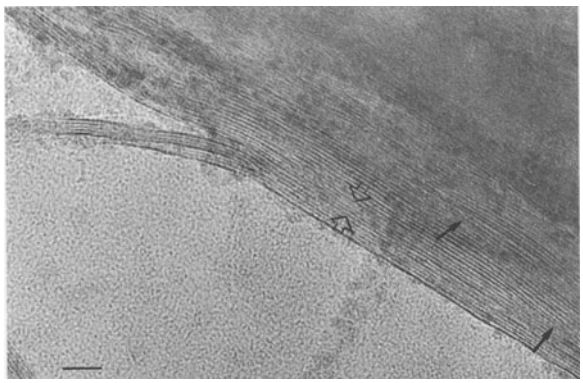

Figure 9. Lattice fringe image with 1 nm spacing throughout. One (or two?) laths have nucleated at a defect on the platelet surface. Numerous growth defects occur (e.g. black arrows) within the particle. Cross fringes (e.g., between open arrows) indicate lattice continuity. The sample is from 2249.4 m and was prepared by ultramicrotomy without fixation of expandable layers. Scale bar = 10 nm.

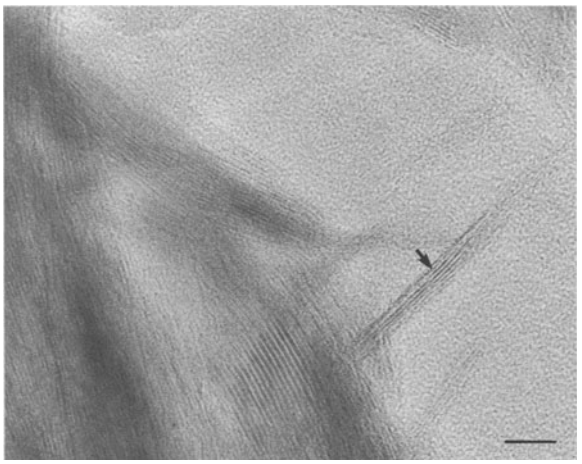

Figure 10. The sub-micrometer particles (e.g., arrow) are inferred to be authigenic from the high angle at which they contact the chlorite (1.4 nm spacing) particle. The sample is from 2271.9 m and was prepared by the method of Tessier, the sub-micron particles with a 1 nm spacing are therefore interpreted as illite. Scale bar = 12 nm.

of their delicate morphology, which indicates that they post-date significant compaction. Both illite and illite-smectite may occur with a lath morphology (Inoue *et al* 1988; Pollastro 1985). The increase in illite and decrease in illite-smectite expandability in the <0.2 μm fraction, compared with the <4 μm fraction, is compatible with an illitic composition for the laths. However the difference in size between 0.2 μm and the laths is too great to make a direct comparison. The 1 nm fringes in laths (Figures 9 and 10) can be interpreted as either 1M illite or mica, or collapsed illite-smectite in a focus condition that shows only the 1 nm fringe, while the 2 nm fringes can be interpreted as either the 2M polytype or R1 illite-smectite (Figure 3). It should be possible to differentiate between the two lath fringe-types on the basis of chemistry. The analyses in Table 1 are for two particles <5 nm thick, which may be laths (analyses 1 and 2), and 2 thicker particles which may be platelets (analyses 3 and 4), these data suggest that both illite (the analysis with higher K and no Na, and illite-smectite (the analyses with Na and <5% K) *may* be present. However the laths are so small that count rates during EDS analysis are very low, and combined with the effects of beam damage, in particular ionization of K and Na, this produces data which are semi-quantitative at best. Consequently, the composition of the laths remains uncertain except in those instances where the smectite spacing has been preserved.

DISCUSSION

Comparison of XRD and TEM data

The correspondence between illite-smectite modal composition as determined by measurement of lattice fringes and compositions determined by XRD reflections indicates that illite-smectite composition is uniform. However it is not clear why the XRD data indicate that the interstratifications are regular, while the HRTEM data indicate that this is so only on the scale of a few structural units, which would not be detected by XRD.

It has been proposed that smectite layers identified by XRD in illite-smectite are in fact the product of interparticle diffraction between overlapping fundamental illite particles (<5 nm), rather than a true interstratified clay (Nadeau *et al* 1984). The TEM identification of interstratified single crystals of illite-smectite in these mudrocks (Figure 3) indicates that illite-smectite is not simply an artifact of XRD preparation. HRTEM and FESEM data indicate that the only particles likely to be <5 nm are the authigenic laths, which are much less abundant than the thicker illite-smectite particles. Semi-quantitative determinations suggest that

Table 1. EDS Analyses of laths (analyses 1 and 2) and platelets (analyses 3 and 4).

Analysis	1	2	3	4
SiO_2	53.8	51.0	53.2	53.8
Al_2O_3	24.0	32.9	31.1	29.9
Fe_2O_3*	9.9	8.2	5.1	4.2
MnO	trace	0.2	0.1	trace
MgO	trace	1.7	1.9	2.3
CaO	2.3	0.1	0.8	1.9
Na_2O	5.6	trace	trace	trace
K_2O	4.4	5.9	7.8	7.9
Total	100.0	100.0	100.0	100.0

* Fe_2O_3 and FeO not differentiated.

https://doi.org/10.1346/CCMN.1995.0430604 Published online by Cambridge University Press

illite-smectite and illite are present in proportions between 2:1 and 1:2 in the <4 μm fraction. While it is accepted that XRD is not a fully quantitative technique, it is reasonable to assume that illite-smectite is very much more abundant than the infrequently observed wispy illite. It is concluded that interparticle diffraction is not the cause of the expandability detected by XRD.

Neoformed illite/illite-smectite

The calculated average temperature (107°C) for the interval of the Forties Sandstone Member described here lies within the temperature range of 80°–120°C quoted for the onset of illitization of smectite (Hower *et al* 1976; Freed 1981; Bruce 1984; Velde *et al* 1986). It is well above the threshold temperature of 60°C given for the North Sea by Small (1993), and below the threshold for extensive illitization suggested by Ehrenberg and Nadeau (1989) for the North Sea Garn Formation. The maximum smectite content of the illite-smectite in the Forties Sandstone Member mudrocks described here is 50%, and shows no clear depth trend over the limited depth range sampled. This evidence does not clearly point to either a detrital or authigenic origin. If the <0.2 μm fraction is at least partially composed of the authigenic laths, then this points to an illite-rich composition for the laths; for example ≤ 20% smectite. A detrital origin is inconceivable for the delicate illitic laths, which implies that they represent the stable illite-smectite composition. The very small proportion of the total rock which is illitic laths, suggests that precipitation is incipient in the Forties Sandstone Member.

Theoretically it should be possible to deduce the modes of illite and illite-smectite formation and particle growth from lattice fringe and structure image data. This is frequently prevented through incomplete data for individual particles as well as the problems of interpretation, summarized above. Structural and chemical alteration during weathering may have modified the stacking of detrital illite-smectite platelets. Consequently it would be unwise to attempt to interpret the mode of illite-smectite formation from the lattice fringe images alone. However, the presence of authigenic laths of illitic composition as overgrowths on detrital (?) platelets has important implications for K/Ar dating of illite. Unless the two generations of clay can be separated (only partially the case with the <0.2 μm fraction described above) any date will be intermediate between the ages of the two clays.

Previous workers have assumed that the authigenic lath-shaped illite observed in the pore space of sandstone does not precipitate in compacted, low porosity, low permeability mudrocks. Yet in the sequence described here such illite may be more abundant in mudrock than in sandstone. A potential source of the requisite ions is present in both lithologies in the form of both leached and unleached K feldspar. Mass balance calculations (Huggett, in press) show that to precipitate the small volume of lath-shaped clay observed, sufficient K, Al and Si would be supplied through feldspar hydrolysis in both lithologies. There is no necessity therefore to invoke either dissolution of detrital illite-smectite, or of authigenic kaolinite, as a source of ions. In an environment which was becoming progressively more closed as compaction reduced pore throat sizes, pH would have risen as hydrolysis reactions used up available acidity. Formation of illite laths (as opposed to platelets) is favored by near neutral solutions (Huang 1990) and may well have occurred as a result of such a sequence of events.

Comparison with previous work

Until recently, X-ray diffraction (XRD) has been the principal investigative tool in mudrock diagenesis, consequently identification of authigenic minerals has been by inference rather than observation. Hower *et al* (1976) concluded that smectite is transformed by a solid state process of cation substitution to form progressively more illitic compositions, with the Al and K both being supplied by external sources. Presumably such a mechanism would result in layers which were part illite, part smectite. These could only be identified in HRTEM images with any certainty where a completely reliable method of fixing the smectite spacing at >1 nm had been utilized. In this study, fringes of variable thickness were infrequently observed in illite-smectite in all samples, and least of all in the samples where the smectite had been fixed.

Boles and Franks (1979) hypothesized that the Al required for the formation of illite layers was derived through dissolution of the smectite itself, rather than from an external source. They suggested that approximately 3 smectite layers are replaced by 2 illite layers, which implies that at least some of the smectite is destroyed and that on an atomic scale this is a dissolution/reprecipitation process. This has since been experimentally verified by conversion of smectite to illite in the absence of an external source of Al (Roberson and Lahann 1981). Many of the illite/illite-smectite particles observed in the present study exhibit fringes which bend around partial fringes (Figure 9). These could be a consequence of 3 smectite layers being replaced by 2 illite layers but again this interpretation would only be unambiguous in samples where the smectite had been fixed with a spacing >1 nm. This feature was not observed in the TEM samples prepared by the method of Tessier, but only in other samples where it could be interpreted as a growth defect within monomineralic clay.

Early studies of the illitization of smectite, including Hower *et al* (1976) and Boles and Franks (1979), were

based on indirect methods of observation, principally XRD. More recent TEM/AEM studies have demonstrated that illite and illite-rich illite-smectite commonly occur as thin subhedral to euhedral thin crystals or packets with 2:1 layers compositionally distinct from those of anhedral, turbostratically layered smectite (Yau *et al* 1983, 1987; Ahn and Peacor 1986; Bautier *et al* 1992). This has been interpreted as indicating a dissolution/recrystallization mechanism for the formation of illite and illite-rich illite-smectite. However the majority of TEM/AEM studies of illite-smectite reaction have been concerned with simple clay assemblages, often from hydrothermal systems, which may differ significantly from clastic sediments undergoing diagenesis. For mudrocks that have a high fluid to rock ratio, a number of authors have observed coexisting illite formed by transformation of smectite, and illite formed from smectite by dissolution-reprecipitation (Pollastro 1985; Yau *et al* 1987; Amouric and Olives 1991; Murakami *et al* 1993). The samples described here are also likely to have experienced a high-fluid rock ratio for mudrocks because the sequence is sandstone dominated. However there is no direct evidence in the TEM data for a transformation origin for the illite-smectite. Although XRD data indicate that the two deepest samples are more illitic, the depth interval sampled is too small for any clear trend in illite-smectite composition to be apparent. Probably the strongest indicators of a detrital origin for the illite-smectite are the plate morphology and the absence of a field-wide correlation between illite-smectite composition and depth. In contrast, neoformed illite-smectite is a very minor but ubiquitous component of these mudrocks, which would result in erroneous K/Ar stable isotope dates for the illite/illite-smectite.

Rosenberg *et al* (1990) suggested that illite chemistry corresponds to particle size. Each discrete illitic phase of a specific thickness has a well constrained chemistry and exists as a singular thermodynamic entity. This model is exceedingly difficult to test in natural systems, such as that described here, where detrital and authigenic illitic clays coexist. It is also difficult to test in the absence of precise geochemical data for individual particles. However it would seem incompatible with the overgrowth mechanism for authigenic illite/illite-smectite formation proposed above. Nor would a simple Ostwald ripening process, such as suggested by Eberl and Środón (1988) be an appropriate mechanism to describe the formation of "overgrowths" of illitic composition. It is conceivable that Ostwald ripening is too simple a theory to be applicable to a mixture of assorted detrital illite-smectite and illite compositions, with discrete and overgrowth neoformed illite/illite-smectite.

The illite/illite-smectite geothermometer

Empirical relationships between illite-smectite composition and temperature have been described for mudrocks from many parts of the world. Useful compilations of relevant data are given by Velde *et al* (1986) and Pollastro (1990). Illite-smectite believed to be neoformed has been reported from mudrocks in a wide range of settings at burial temperature of between 50°C and 150°C (Hoffman and Hower 1979; Freed 1981; Jennings and Thompson 1986; Pearson and Small 1988). Through a synthesis of published data, including graphs of temperature plotted against % smectite in illite-smectite cross-plots, Velde *et al* (1986) demonstrated that the rate of illitization was dependent upon geothermal gradient. Using these graphs and the present day average measured reservoir temperature of 107°C (and therefore a present day geothermal gradient of 43°C/km) for the Forties Sandstone Member we have compared the composition of authigenic illite-smectite from a range of settings with that reported here from the Forties Sandstone Member. In areas of low geothermal gradient (30°–40°C/km) such as the Gulf Coast, a wide range in authigenic illite-smectite composition, from 20% to 70% smectite, is compatible with a temperature of 107°C (Freed 1981; Bruce 1984). In areas of higher geothermal gradient (around 100°C/km), such as in the Niger Delta and the Colorado River Delta, the range is 45–65% smectite in illite-smectite, at the same temperature (Velde *et al* 1986; Jennings and Thompson 1986). A broad range of stable illite-smectite compositions is therefore predicted for the Forties Sandstone Member. This predicted range encompasses the measured range of compositions. The absence of any clear trend toward a more illitic composition with depth over the limited depth range sampled, or of any change in composition across the oil-water contact zone, does not support an authigenic origin for the Forties Sandstone Member illite-smectite. While the two deepest samples do contain more illitic illite-smectite than the rest, it would be unwise to deduce an authigenic origin on the basis of these data alone. The only irrefutably authigenic "illitic" clay is the lath-shaped overgrowths on illite or illite-smectite platelets. For illite-smectite to be a true geothermometer, it must be in chemical and thermal equilibrium. Where a progressive change with depth can be identified, this may be a valid assumption. However, for the Forties Sandstone Member, the stable composition is represented by the thin laths of authigenic illitic clay, which are present in amounts too small to have been detected by XRD alone. Any estimate of maximum burial temperature based on illite-smectite mineral composition would probably have been in error as a consequence.

SUMMARY

Detrital illite and illite-smectite platelets, plus authigenic illitic laths (R1), coexist within the 70 m depth interval of the Sele formation mudrocks which have been examined in this study. Many lattice fringes show

2 nm super lattice structures, but only where smectite layers have been fixed at >1 nm has R1 illite-smectite been identified with confidence. The increase in proportion of illite to smectite layers observed in lattice fringes in the two deepest samples mirrors the increase identified from XRD data. However, whereas the XRD indicates a regular interstratification, the TEM data only shows regular interstratification over a distance of a few layers. This depth change is attributed to a change in the nature of the detrital illite source rather than to diagenetic alteration.

Where smectite layers have been fixed at >1 nm R1 illite-smectite laths have been identified with confidence, consequently both illite-smectite and illite laths may coexist. The authigenic illitic laths differ from previous reported occurrences in that they appear to have formed as discrete particles and overgrowths, without being preceded by progressive illitization of illite-smectite.

ACKNOWLEDGMENTS

With the exception of the analytical TEM, which was carried out at the Micro Structural Studies Unit at the University of Surrey, this work was carried out while the author was visiting the Center for Microscopy and Microanalysis at the University of Queensland, Australia.

REFERENCES

Ahn, J. H., and D. R. Peacor. 1986. Transmission and analytical electron microscopy of the smectite-to-illite transition. *Clays & Clay Miner.* **34**: 165–179.

Amouric, M., and J. Olives. 1991. Illitization of smectite as seen by high-resolution electron microscopy. *Eur. J. Mineral.* **3**: 831–835.

Baños, J. O., M. Amouric, C. De Fouquet, and A. Baronnet. 1983. Interlayering and interlayer slip in biotite as seen by HRTEM. *Amer. Mineral.* **68**: 754–758.

Bautier, M. D., D. R. Peacor, and J. R. O'Niel. 1992. Smectite-illite transition in Barbados accretionary wedge sediments: TEM and AEM evidence for dissolution/crystallisation at low temperature. *Clays & Clay Miner.* **38**: 33–46.

Boles, J. R., and S. G. Franks. 1979. Clay diagenesis in Wilcox sandstones of southwest Texas. *J. Sed. Petrol.* **49**: 55–70.

Bruce, C. H. 1984. Smectite dehydration—Its relation to structural development and hydrocarbon accumulation in the Northern Gulf of Mexico basin. *Amer. Assoc. Petrol. Geol. Bull.* **68**: 673–683.

Burton, W. K., N. Cabrera, and F. C. Frank. 1951. The growth of crystals and the equilibrium structure of their faces. *Phil. Trans. Royal Soc.* **243**: 299–358.

Buseck, P. R., and S. Ijima. 1974. High resolution electron microscopy of silicates. *Amer. Mineral.* **59**: 1–21.

Eberl, D. D., and J. Sródon. 1988. Ostwald ripening and interparticle diffraction effects for illite crystals. *Amer. Mineral.* **73**: 1335–1345.

Ehrenberg, S. N., and P. H. Nadeau. 1989. Formation of diagenetic illite in sandstones of the Garn Formation, Haltenbanken area, mid-Norwegian continental shelf. *Clay Miner.* **24**: 233–253.

Freed, R. L. 1981. Shale mineralogy and burial diagenesis of the Frio and Vicksburg Formations in two geopressured wells, McAllen Ranch area, Hidalgo County, Texas. *Trans. Gulf Coast Assoc. Geol. Soc.* **31**: 189–293.

Glassman, J. R. 1992. The fate of feldspars in the Brent Group reservoirs, North Sea: a regional synthesis of diagenesis in shallow, intermediate and deep burial environments. In *Geology of the Brent Group.* A. C. Morton, R. S. Haszeldine, M. R. Giles, and S. Brown, eds. London: The Geological Society, 329–350.

Guthrie, G. D. Jr., and D. R. Veblen. 1989. High resolution transmission electron microscopy of mixed layer illite/smectite: Computer simulations. *Clays & Clay Miner.* **37**: 1–11.

Guthrie, G. D. Jr., and D. R. Veblen. 1990. Interpreting one-dimensional, high-resolution transmission electron micrographs of sheet silicates by computer simulation. *Amer. Mineral.* **75**: 276–288.

Hoffman, J., and J. Hower. 1979. Clay mineral assemblages as low grade metamorphic geothermometers: Application to the thrust faulted disturbed belts of Montana. U.S.A. SEPM Special Publication. **26**: 55–79.

Hower, J., E. V. Eslinger, M. E. Hower, and E. A. Perry. 1976. Mechanisms of burial metamorphism of argillaceous sediments: 1 Mineralogical and chemical evidence. *Geol. Soc. Amer. Bull.* **897**: 725–737.

Huang, W. L. 1990. Experimental illitization of illite and recrystallization of illite. In *Programme and Abstracts, Research Conference on Phyllosilicates as Indicators of Very Low Grade Metamorphism and Diagenesis.* Manchester: IGCP, 10.

Huggett, J. M. 1989. Scanning electron microscope and X-ray diffraction investigations of mudrock fabrics, textures and mineralogy. *Scanning Microscopy* **3**: 99–109.

Huggett, J. M. 1992. Petrography, mineralogy and diagenesis of overpressured Tertiary and Late Cretaceous mudrocks from the East Shetland Basin. *Clay Miner.* **27**: 487–506.

Huggett, J. M. Diagenesis in a Tertiary sandstone-mudrock sequence from the Central North Sea, U.K. (in press).

Inoue, A., H. Kohyama, R. Kitagawa, and T. Watanabe. 1987. Chemical and morphological evidence for the conversion of smectite to illite. *Clays & Clay Miner.* **35**: 111–120.

Inoue, A., B. Velde, A. Meunier, and G. Touchard. 1988. Mechanism of illite formation during smectite-to-illite conversion in a hydrothermal system. *Amer. Mineral.* **73**: 1325–1334.

Jennings, S., and G. R. Thompson. 1986. Diagenesis in Plio-Pleistecene sediments in the Colorado River delta, southern California. *J. Sed. Petrol.* **56**: 89–98.

Keller, W. D., R. C. Reynolds, and A. Inoue. 1986. Morphology of clay minerals in the smectite-to-illite conversion series by scanning electron microscopy. *Clays & Clay Miner.* **34**: 187–197.

Lee, J. H., J. H. Ahn, and D. R. Peacor. 1985. Textures in layered silicates: Progressive changes through diagenesis and low-temperature metamorphism. *J. Sed. Petrol.* **55**: 532–540.

Murakami, T., T. Sato, and T. Watanabe. 1993. Microstructure of interstratified illite/smectite at 123 K: a new method for HRTEM examination. *Amer. Mineral.* **78**: 465–468.

Nadeau, P. H., J. M. Tait, W. J. McHardy, and M. J. Wilson. 1984. Interstratified XRD characteristics of physical mixtures of elementary clay particles. *Clay Miner.* **19**: 67–76.

O'Brien, N. E., and R. M. Slatt. 1990. *Argillaceous Rock Atlas.* New York: Springer Verlag, 141 pp.

Peacor, D. R. 1992. Diagenesis and low-grade metamorphism of shales and slates. In *Reviews in Mineralogy 27*

Mineral Reactions at the Atomic Scale: Transmission Electron Microscopy. P. R. Buseck, ed. Washington: Miner. Soc. Amer., 335–379.

Pearson, M., and J. S. Small. 1988. Illite-smectite diagenesis and palaeotemperatures in Northern North Sea Quaternary to Mesozoic shale sequences. *Clay Miner.* **23**: 109–132.

Pollastro, R. M. 1985. Mineralogical and morphological evidence for the formation of illite at the expense of illite/smectite. *Clays & Clay Miner.* **33**: 265–274.

Pollastro, R. M. 1990. The illite/smectite geothermometer—Concepts, methodology and application to basin history and hydrocarbon generation. In *Applications of Thermal Maturity Studies to Energy Exploration.* V. F. Nuccio and C. E. Barker, eds. Denver: Rocky Mountain Section, SEPM, 1–18.

Reynolds, R. C. Jr., and J. Hower. 1970. The nature of interlayering in mixed layer illite-montmorillonites. *Clays & Clay Miner.* **18**: 165–177.

Reynolds, R. C. Jr. 1985. NEWMOD© *A Computer Program for the Calculation of One-Dimensional Diffraction Patterns of Mixed-Layer Clays.* R. C. Reynolds Jr. 8 Brook Drive, Hanover, New Hampshire.

Roberson, H. E., and R. W. Lahann. 1981. Smectite to illite conversion states: Effects of solution chemistry. *Clays & Clay Miner.* **29**: 129–135.

Rosenberg, P. E., J. A. Kittrick, and S. U. Aja. 1990. Mixed-layer illite/smectite: A multiphase model. *Amer. Mineral.* **75**: 1182–1185.

Small, J. S. 1993. Experimental determination of the rates of precipitation of authigenic illite and kaolinite in the presence of aqueous oxalate and comparison to the K/Ar ages of authigenic illite in reservoir sandstone. *Clays & Clay Miner.* **41**: 191–208.

Środón, J. 1980. Precise identification of illite/smectite interstratifications by X-ray powder diffraction. *Clays & Clay Miner.* **28**: 401–411.

Srodon, J., C. Andreoli, F. Elsass, and M. Robert. 1990. Direct high resolution electron microscopic measurement of expandability of mixed layer illite/smectite in bentonite rock. *Clays & Clay Miner.* **38**: 373–379.

Vali, H. and H. M. Köster. 1986. Expanding behaviour, structural disorder, regular and random irregular interstratification of 2:1 layer-silicates studied by high resolution images of transmission electron microscopy. *Clay Miner.* **21**: 827–859.

Veblen, D. R., G. D. Guthrie, K. J. T. Livi, and R. C. Reynolds Jr. 1990. High resolution transmission electron microscopy and electron diffraction of mixed layer illite/smectite: Experimental results. *Clays & Clay Miner.* **38**: 1–13.

Velde, B., T. Suzuki, and E. Nicot. 1986. Pressure-temperature-composition of illite/smectite mixed-layer minerals: Niger Delta mudstones and other examples. *Clays & Clay Miner.* **34**: 435–441.

Yau, Y.-C., J. H. Lee, D. R. Peacor, and S. D. McDowell. 1983. TEM study of illite diagenesis in shale of Salton Sea geothermal field, California. In *Program and Abstracts, 20th Annual Meeting Clay Minerals Society,* 42.

Yau, Y-C., D. R. Peacor, and S. D. McDowell. 1987. Smectite-to-illite reactions in Salton Sea shales: A transmission and analytical electron microscopy study. *J. Sed Petrol.* **57**: 335–342.

(Received 16 August 1994; accepted 17 April 1995; Ms. 2562)